New high spin states and band termination in ^{83}Y and ^{84}Zr

T. D. Johnson and A. Aprahamian
University of Notre Dame, Notre Dame, Indiana 46556

C. J. Lister, D. J. Blumenthal, and B. Crowell
Argonne National Laboratory, Argonne, Illinois 60439

P. Chowdhury
University of Massachusetts, Lowell, Massachusetts 01854

P. Fallon and A. O. Machiavelli
Lawrence Berkeley National Laboratory, Berkeley, California 94720

(Received 12 August 1996)

The gamma decay of high spin yrast states in ^{83}Y up to $I^{\pi}=59/2^{+}$ and $53/2^{-}$ have been observed using the reaction ^{58}Ni(^{29}Si,3p) at 110 MeV and the Gammasphere Early Implementation Array. The level scheme has been substantially extended due to the observations of several new transitions in all of the bands. A sequence of transitions feeding into the positive parity yrast band above $I^{\pi}=47/2^{+}$ seems to be consistent with a noncollective oblate structure expected at these high spins. A similar cascade is found in the data for ^{84}Zr. A new forking of the favored negative parity band is found which may be due to neutron alignment polarizing the core to a different shape. This suggests that the ''isomeric'' band in ^{83}Y, for which one more connecting transition was found, is of a similar nature to other high-K bands found in this region. Lifetime measurements in the unfavored negative parity band are consistent with cranking calculations which predict a nearly oblate shape with a deformation parameter $\beta_2\approx 0.2$. A qualitative analysis of line shapes at very high spins suggests the persistence of collectivity in the yrast sequence to the highest excitations seen. [S0556-2813(97)03603-0]

PACS number(s): 21.10.Re, 21.60.Ev, 23.20.Lv, 27.50.+e

I. INTRODUCTION

Large deformation, reduction in pairing, and rapid alignment of nucleons characterize nuclei in the neutron deficient $A\approx 80$ region. The low level density, the existence of strongly shape-driving orbitals near the Fermi surface, and large deformed shell gaps all lead to a wealth of interesting shape polarizing phenomena at all spins. Some of the nuclei near the $N,Z=38$ gap have large ground state ($\beta_2=0.4$) prolate deformations while recent experiments [1–6] have revealed ''superdeformed configurations'' in nuclei with their neutron Fermi surface near $N=44$. The motivation of the present study was to search for the predicted highly deformed structures and possible band termination effects in the $N=44$ isotones ^{84}Zr and ^{83}Y by means of Doppler shift attenuation (DSA) lifetime measurements and $\gamma\gamma\gamma$ coincidences. In addition, new information was expected, especially on the lifetimes of non-yrast states which should clarify their shapes and the aligned-particle configurations that cause them.

The $N=44$ isotope ^{83}Y has been investigated in detail by several groups [7–10]. The level structure was known to tentative spins and parities $49/2^{+}$ and $45/2^{-}$. Comparisons with the crossing frequencies predicted by cranking calculations [10] suggest that the first backbend occurs at $\hbar\omega=0.55$ MeV and that it is due to a neutron alignment. A similar comparison for the negative parity unfavored band indicated an initial $g_{9/2}$ proton alignment followed by a $g_{9/2}$ neutron alignment. Lifetime measurements [5,11] demonstrated that the structure of the positive parity $\alpha=+1/2$ band is consistent with a large prolate deformation which decreases with increasing spin. A somewhat less deformed triaxial shape was predicted [10] for the unfavored signature partner. Calculations presented in Ref. [10] also predicted the presence of highly deformed prolate structures with $\beta_2\approx 0.43$, however such a structure was not found in this experiment [10].

II. EXPERIMENT AND ANALYSIS PROCEDURE

The reaction ^{58}Ni(^{29}Si,3p) at 110 MeV was used to populate high spin states in ^{83}Y. The experiment was performed at the 88 inch Cyclotron at Lawrence Berkeley National Laboratory using the Early Implementation Gammasphere array [12] with 33 detectors. Two experiments were carried out using thin and thick targets. The thin target experiment consisted of three stacked ^{58}Ni targets with an average thickness of 341 $\mu g/\mathrm{cm}^2$. The thick target experiment consisted of a 788 $\mu g/\mathrm{cm}^2$ foil on a 15.3 mg/cm^2 Au backing and tilted 45° relative to the beam axis. A minimum of threefold coincidences between Compton-suppressed Ge detectors were required and 2.9×10^8 triple events were collected for the thin target experiment and 2.3×10^8 events for the thick target experiment. The recoil velocity averaged to $v/c=0.0280$ via the calibration of known lines in ^{84}Zr from the thin target experiment.

The analysis was done by first presorting the raw events to specially formatted tapes. Thin target data were further sorted into a Hackman-Kuehner [14] symmetrized cube. Projections from the cube were made using ''gator'' [15] and

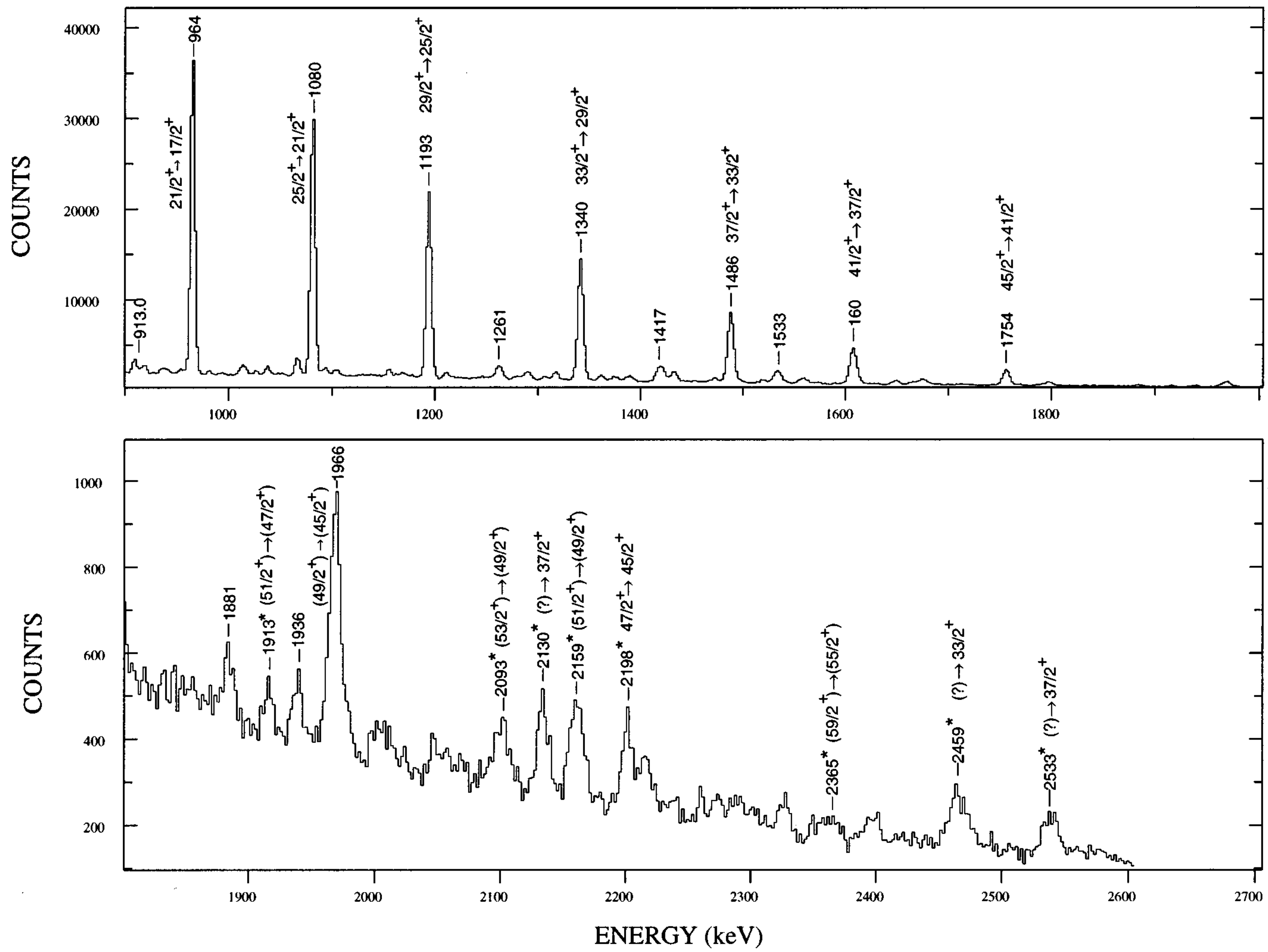

FIG. 1. Spectrum of ^{83}Y from Early Implementation Gammasphere based on double-gating with combinations of the low-lying transitions. Some of the new transitions are labeled with an asterisk.

''butcher'' [15] software. The background subtraction procedure used the FUL method described in Ref. [16]. The data were also sorted into angle dependent primary gated matrices from which secondary gates were used to project out spectra for specific angles, using the codes SMATNL [13] and GG [13]. The angle dependent matrices from the thin target data were used to determine empirical asymmetry ratios that are related to directional correlation ratios of oriented nuclei (DCO). To maximize statistics, the matrices combined all forward angle (relative to the beam axis) detectors against the six 90° detectors, and similarly for the back angle detectors. The ratios were then checked against known multipolarities. The thick target data were similarly sorted into angle dependent primary gated matrices to project out spectra for line shape analysis. To maximize statistics, spectra from the five detectors at 32° and the five detectors at 37° were combined to an average angle of 35° for the line shape analysis.

III. THE LEVEL SCHEME

A. Positive parity bands

A spectrum showing transitions connected to the favored positive parity band is shown in Fig. 1. The spectrum was generated by combining spectra from different double gates of all known transitions within the ground state band. New transitions are marked with an asterisk.

The intensities of all transitions which could be measured are compiled in Tables I and II along with empirical angular asymmetry ratios determined from the primary energy gated angle dependent matrices. The relative intensities were determined from gating on all lower transitions, efficiency corrected, and normalized to the same lines used in Ref. [10], for comparison purposes. Intensities for the lowest transitions from Ref. [10] are also presented for completeness. To determine asymmetry ratios, pure $E2$ transitions were used for both primary and secondary gating conditions. The empirically determined asymmetry ratios are related to the theoretical DCO ratios. They provide a differentiation between stretched quadrupole and dipole transitions and also $\Delta I=0$ dipole transitions. Letting γ_1 denote the primary gating transition, they are defined as

$$R_{\text{asym}}=\frac{Y(\gamma_2 \text{ at } \theta_1 \text{ gated by } \gamma_3 \text{ at } \theta_2)}{Y(\gamma_3 \text{ at } \theta_2 \text{ gated by } \gamma_2 \text{ at } \theta_1)} \tag{1}$$

with Y denoting the intensity θ_1, all angles forward or back-

TABLE I. Energies, intensities, and R_{asym} ratios for the $\pi=+$ bands in ^{83}Y.

E_x(keV)	E_γ (keV)	I_i^π	I_f^π	Y_{rel}^γ	R_{asym}
595.3	595.3	$13/2^+$	$9/2^+$	962(70) [a]	–
1406.9	811.6	$17/2^+$	$13/2^+$	800(70) [a]	–
2371.3	964.4	$21/2^+$	$17/2^+$	626(26)	1.05(7)
3451.6	1080.3	$25/2^+$	$21/2^+$	433(22)	0.97(8)
4644.4	1192.8	$29/2^+$	$25/2^+$	284(18)	1.04(11)
5984.7	1340.3	$33/2^+$	$29/2^+$	171(14)	0.94(8)
7471.2	1486.5	$37/2^+$	$33/2^+$	100(11)	1.04(11)
8443.3	2458.6	–	$33/2^+$	2.2(19)	–
9077.0	1605.8	$41/2^+$	$37/2^+$	68(9)	1.10(15)
9600.8	2129.6	–	$37/2^+$	2.8(18)	–
10004	2533	–	$37/2^+$	–	–
10830.9	1753.9	$45/2^+$	$41/2^+$	23(5)	1.15(30)
12796.6	1965.7	$(49/2^+)$	$45/2^+$	6(3)	–
13029	2198	$47/2^+$	$45/2^+$	2(1)	0.37(22)
13043	2212	$(47/2^+)$	$45/2^+$	1.8(14)	0.83(43)
14890.5	2093.9	$(53/2^+)$	$(49/2^+)$	1.0(9)	–
14956	2159	$(51/2^+)$	$(49/2^+)$	2.0(15)	–
	1913	$(51/2^+)$	$(47/2^+)$	1.0(9)	–
17096	2154	$(55/2^+)$	$(51/2^+)$	1.3(12)	–
19461	2365	$(59/2^+)$	$(55/2^+)$	1.0(9)	–
145.4	145.4	$7/2^+$	$9/2^+$	–	–
738.2	592.8	$11/2^+$	$9/2^+$	–	–
	736.8	$11/2^+$	$7/2^+$	–	–
1532.5	794.3	$15/2^+$	$11/2^+$	–	–
	937.4	$15/2^+$	$13/2^+$	–	–
2429.0	896.5	$25/2^+$	$21/2^+$	132(10)	–
	1024.0	$19/2^+$	$17/2^+$	12(5)	–
3395.4	966.4	$23/2^+$	$19/2^+$	100(12)	–
	1025.2	$23/2^+$	$21/2^+$	8.7	–
4487.5	1092.1	$27/2^+$	$23/2^+$	68(8)	–
	1037.0	$27/2^+$	$25/2^+$	12(4)	0.54(13)
5747.4	1259.9	$(31/2^+)$	$27/2^+$	59(8)	–
	1103.1	$(31/2^+)$	$29/2^+$	5(1)	–
7178.6	1431.2	$(35/2^+)$	$(31/2^+)$	40(8)	–
	1195.7	$(35/2^+)$	$33/2^+$	–	–
8712.5	1533.9	$(39/2^+)$	$(35/2^+)$	38(3)	–
10360.0	1647.5	$(43/2^+)$	$(39/2^+)$	12(4)	–
12244.9	1884.9	$(47/2^+)$	$(43/2^+)$	10(4)	–
14029.3	1784.4	$(51/2^+)$	$(47/2^+)$	9(4)	–

[a]Intensities from Ref. [10].

TABLE II. Energies and intensities for the $\pi=-,\alpha=+1/2$ band in ^{83}Y.

E_x(keV)	E_γ (keV)	I_i^π	I_f^π	Y_{rel}^γ
814.2	647.1	$9/2^-$	$5/2^-$	106(8) [a]
1566.3	752.1	$13/2^-$	$9/2^-$	187(14) [a]
2406.1	839.8	$17/2^-$	$13/2^-$	110(9) [a]
3315.5	909.4	$(21/2^-)$	$17/2^-$	139(14)
4342.1	1026.6	$(25/2^-)$	$(21/2^-)$	119(11)
5503.4	1161.3	$(29/2^-)$	$(25/2^-)$	99(10)
6677.6	1174.2	$(33/2^-)$	$(29/2^-)$	43(7)
6781.6	1278.2	$(33/2^-)$	$(29/2^-)$	29(6)
7922.3	1244.7	$(37/2^-)$	$(33/2^-)$	26(6)
8109.6	1328.0	$(37/2^-)$	$(33/2^-)$	17(5)
9335.5	1413.2	$(41/2^-)$	$(37/2^-)$	22(5)
9641	1531	$(41/2^-)$	$(37/2^-)$	5(2)
10930.1	1594.6	$(45/2^-)$	$(41/2^-)$	10(4)
11268	1627	$(45/2^-)$	$(41/2^-)$	–
12729.3	1799.2	$(49/2^-)$	$(45/2^-)$	2(1)
14779	2041	$(53/2^-)$	$(49/2^-)$	2(1)

[a]Intensities from Ref. [10].

ward, relative to the beam axis, and $\theta_2=90°$. With the chosen geometry, a check was made against known transitions, the asymmetry ratios are $R_{asym}=1.0$ for $\Delta I=2$ or $\Delta I=0$ transitions and $R_{asym}\approx 0.5$ for stretched $\Delta I=1$ dipole transitions.

The level scheme depicted in Fig. 2 was constructed from double gated spectra, similar to the one shown in Fig. 1.

We adopt the band level labeling scheme used in Ref. [10], namely that the positive parity favored signature ($\pi=+,\alpha=+1/2$) and the positive parity unfavored signature ($\pi=+,\alpha=-$) bands shall be referred to as the $(+,+)$ and $(+,-)$ bands, respectively. Similar labeling is used for the negative parity bands. Several of the new transitions in the level scheme can be seen in Fig. 2. In addition to the decays which have been located, several new transitions belonging to this nucleus were found, which could not be unambiguously placed. Several problems in the assignment were encountered: the width of high energy transitions arising from recoil into vacuum, the presence of close-lying doublets, and the irregular sequences of transitions at higher spins. For example, the 2093 keV transition can barely be distinguished on the left shoulder of the 2098 keV line in Fig. 1. Triple coincidence spectra show that the 2098 keV line is in coincidence with several members in the yrast band, but the poor statistics obtained when gating with transitions higher in the band do not permit a firm placement. However, those spectra do show an increasing dominance of the left shoulder at 2093 keV, and spectra based on gate combinations of high-lying lines (above $37/2^+$) coincident with lower-lying transitions show a clear centroid at 2093 keV with no peak or shoulder centered at 2098 keV. These double gated spectra also show a complete disappearance of the high energy transitions at 2130, 2533, and 2459 keV. Careful gating selections, using transitions systematically up the band in combination with the 595 and 811 keV lines, show that these directly populate the $37/2^+$ and $33/2^+$ states. Angular asymmetry ratios could not be determined for these lines due to the low statistics in the angle dependent matrices when using only clean gates. An asymmetry ratio was measured for the 2198 keV line, and although the error bars are large, they are still consistent with a $\Delta I=1$ transition. The similarity in energy and placement for the 2212 keV peak, also populating the $(45/2^+)$ state, suggest that it is also a $\Delta I=1$ transition, however, the larger uncertainties in the asymmetry ratio only permit a tentative assignment. The 2159 keV line was located and found to be a doublet when it was used in gating combinations with other members of the yrast cascade. The energy centroid of its doublet partner is clearly established to be 2154 keV. This placement is also supported by the 1913 keV transition in coincidence with the 2154 keV transition. A spin-parity assignment of $51/2^+$ is tentatively assigned to the 14 956 keV level since the se-

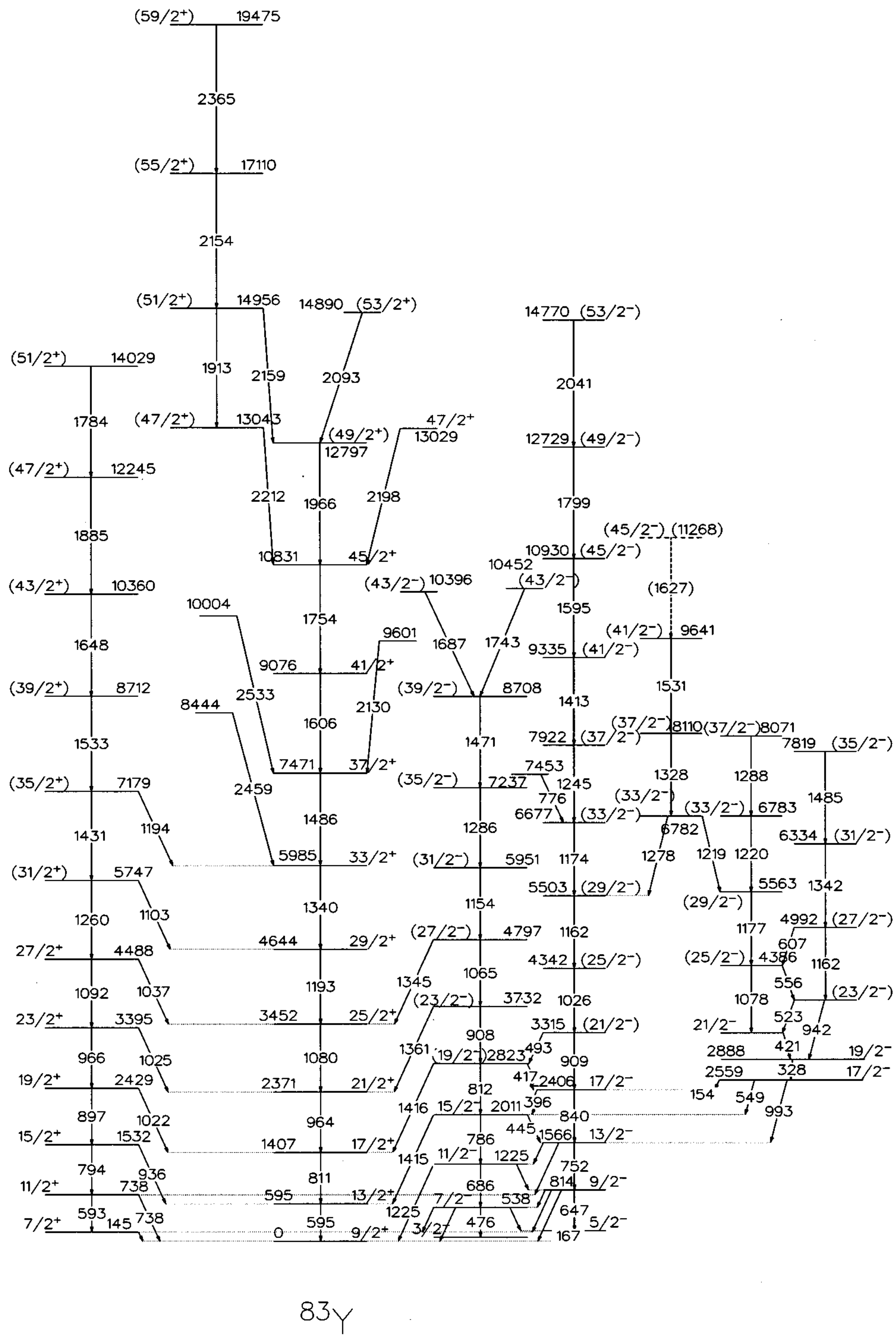

FIG. 2. Partial level scheme of the ^{83}Y nucleus based on the present experiment. Not shown is another side band presented in Ref. [10] and several side transitions.

quence of the three new transitions extending to 19 475 keV appears to be regular in character, although the doublet nature of the 2159 keV line and the weak 1913 keV line do not permit a reasonable estimate of the asymmetry ratio. The pattern of two high energy ($>$ 2 MeV) γ rays depopulating from two levels feeding into the yrast levels, with a connecting transition between them is similar to the pattern observed recently [2] in ^{84}Zr. A more careful search in the current data led to the additional transitions to extend this sequence in ^{84}Zr. In fact, two new transitions were found in ^{84}Zr as a result of this search and their placement is shown in Fig. 3, together with a partial level scheme of ^{83}Y for comparison. It is interesting that the observed feeding pattern into the ground state band for both nuclei are very similar.

The unfavored $(+,-)$ band is extended by two transitions to $(51/2^+)$. The placement of the 1784 keV line feeding into the 12245 keV state is supported by its intensity. Although, the tabulated intensities of the 1885 keV and the 1784 keV lines are equal, individual gate combinations show a higher intensity for the 1885 keV line. Highfold data were ex-

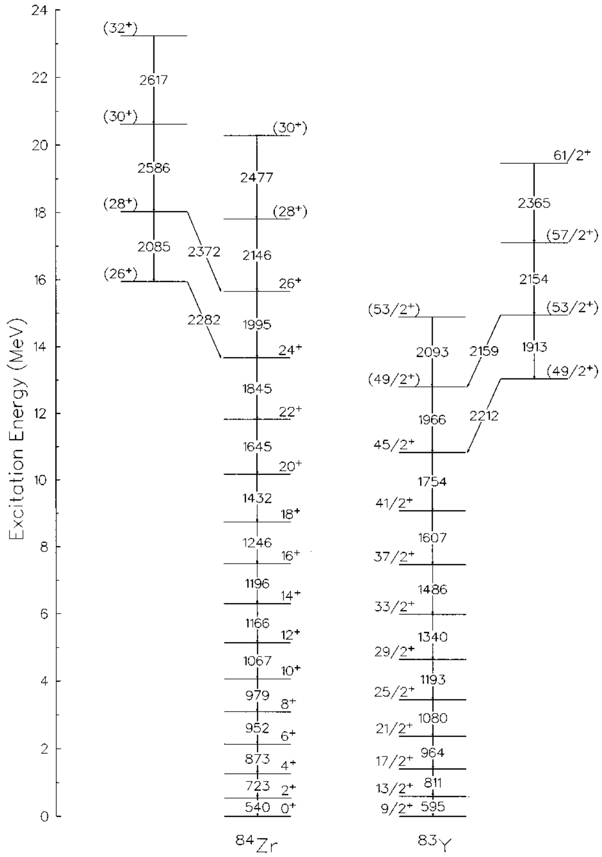

FIG. 3. A partial level scheme comparing the new side-feeding cascade found in ^{84}Zr with the cascade found in the ^{83}Y isotone.

tremely useful in the placement of γ rays, many of which were doublets. The 964 and 966 keV lines were sufficiently resolved for gating purposes, and by double gating using both the 811 and the 966 keV lines, along with the 964 and the 1093 keV coincidence gates, we found the 1022 and 1025 keV connecting transitions. Normalized intensities for these lines could not be determined. However, branching ratios were established by using the populating transitions for the gating conditions and are shown in Table III, in connection with lifetime measurements.

Recent reports [1,2], announcing the discovery of superdeformed bands in ^{84}Zr and ^{83}Sr motivated a search for superdeformed structures in ^{83}Y. A band finding routine [15] was used to search the entire cube for possible candidates for superdeformed band structures. Several candidates were found. One of the candidate bands begins with a 1526 keV line, already known as the first transition for the superdeformed band in ^{84}Zr. The energy level spacings from the search also matched those from Ref. [2]. Using the 1526 keV line in various gating combinations confirmed coincidences with the main yrast band in ^{84}Zr. However, statistics were too poor to establish further coincidences with any other member of the superdeformed band. Another candidate for an initial transition from a superdeformed band was found at 1556 keV. Very similar to the situation in ^{84}Zr, gates with this line revealed coincidences with transitions in the yrast band of ^{83}Y. However, due to very low statistics, no coincidences could be confirmed using higher-lying members of the band suggested by the band searching routine. A careful manual search of regions in the neighborhood of the lines found in the band search could confirm no further coincidences. The current experiment at 110 MeV was 18 MeV lower than that in Ref. [2]. It seems that the lower energy of the present experiment resulted in a much weaker population of superdeformed bands.

B. Negative parity bands

Several new transitions have been added to the negative parity bands. It was not possible to ascertain all the asymme-

TABLE III. Lifetimes, transition strengths, and quadrupole moments in ^{83}Y.

E_γ (keV)	I_i^π	I_f^π	Branching ratio (%)	τ (ps)	τ [a] (ps)	$B(E2)$ (W.u.)	$B(M1)$ (μ_N^2)	$\lvert Q_t \rvert$ (e b)
595.3	$13/2^+$	$9/2^+$	100	–	$7.80\,(^{14}_{14})$	$65\,(^{7}_{5})$		$3.23\,(^{34}_{26})$
811.6	$17/2^+$	$13/2^+$	100	–	$1.39\,(^{15}_{15})$	$78\,(^{4}_{4})$		$2.79\,(^{16}_{14})$
964.4	$21/2^+$	$17/2^+$	100	–	$0.62\,(^{10}_{10})$	$74\,(^{7}_{5})$		$2.47\,(^{23}_{18})$
1080.3	$25/2^+$	$21/2^+$	100	–	$0.38\,(^{8}_{8})$	$68\,(^{8}_{6})$		$2.26\,(^{28}_{21})$
1192.8	$29/2^+$	$25/2^+$	100	$0.28\,(^{5}_{4})$	$0.29\,(^{7}_{7})$	$56\,(^{5}_{5})$		$1.99\,(^{16}_{16})$
1340.3	$33/2^+$	$29/2^+$	100	$0.32\,(^{13}_{10})$	< 0.39	$27\,(^{6}_{4})$		$1.35\,(^{29}_{20})$
1486.5	$37/2^+$	$33/2^+$	100	$0.07\,(^{4}_{3})$	–	$75\,(^{25}_{16})$		$2.22\,(^{75}_{48})$
1605.8	$41/2^+$	$37/2^+$	100	$0.02\,(^{8}_{1})$	–	$182\,(^{78}_{105})$		$3.43\,(^{148}_{198})$
1753.9	$45/2^+$	$41/2^+$	100	$0.02\,(^{8}_{1})$	–	$115\,(^{48}_{63})$		$2.70\,(^{112}_{149})$
1965.7	$(49/2^+)$	$45/2^+$	100	$0.01\,(^{5}_{1})$	–	$129\,(^{7}_{76})$		$2.84\,(^{15}_{168})$
966.4	$23/2^+$	$19/2^+$	92(1)	$0.62\,(^{16}_{13})$	–	$59\,(^{7}_{6})$		$2.16\,(^{27}_{23})$
1025.2	$23/2^+$	$21/2^+$	8(1)	–	–	–	$0.01\,(^{1}_{05})$	
1092.1	$27/2^+$	$23/2^+$	75(7)	$0.29\,(^{9}_{11})$	–	$57\,(^{15}_{7})$		$2.03\,(^{55}_{26})$
1037.0	$27/2^+$	$25/2^+$	15(7)	–	–	–	$0.03\,(^{1}_{2})$	–
1259.9	$(31/2^+)$	$27/2^+$	92(2)	$0.29\,(^{11}_{10})$	–	$40\,(^{8}_{6})$		$1.66\,(^{33}_{23})$
1103.1	$(31/2^+)$	$29/2^+$	8(2)	–	–	–	$0.01\,(^{1}_{05})$	–
1431.2	$(35/2^+)$	$(31/2^+)$	100	< 0.34[b]	–	> 18		$1.10\,(^{16}_{23})$

[a]Taken from Ref. [11].

[b]Not corrected for feeding.

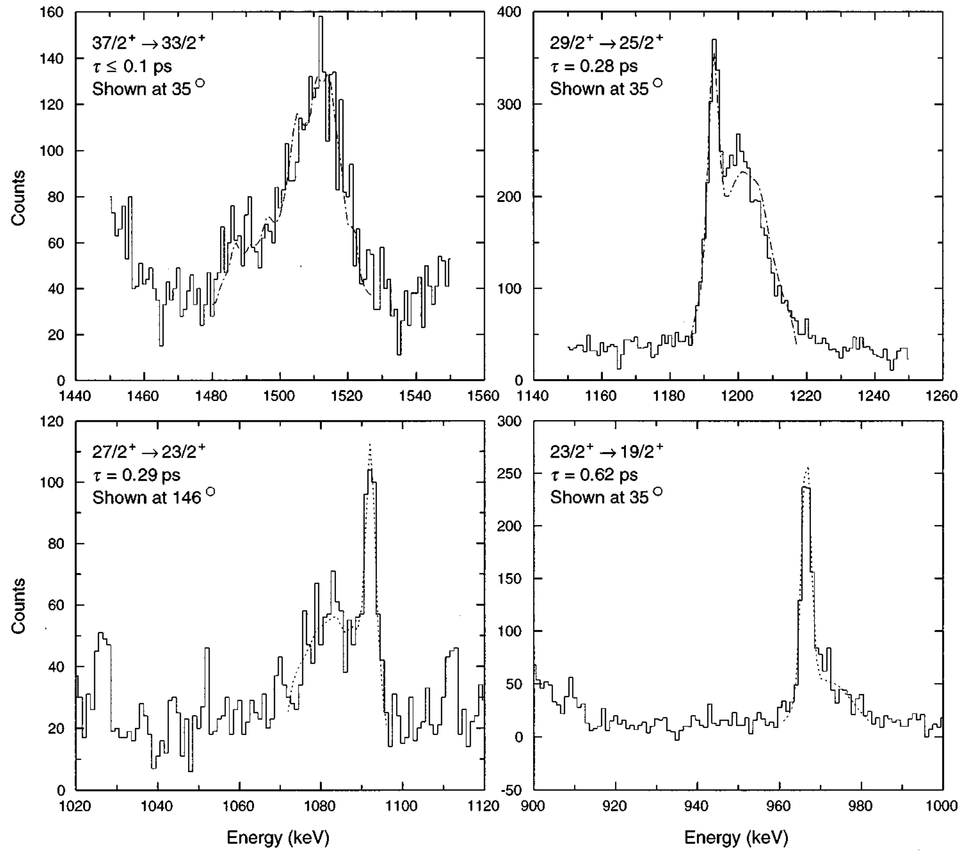

FIG. 4. Line shapes from the present experiment. The line shapes generated from LILIFIT are shown as dashed lines.

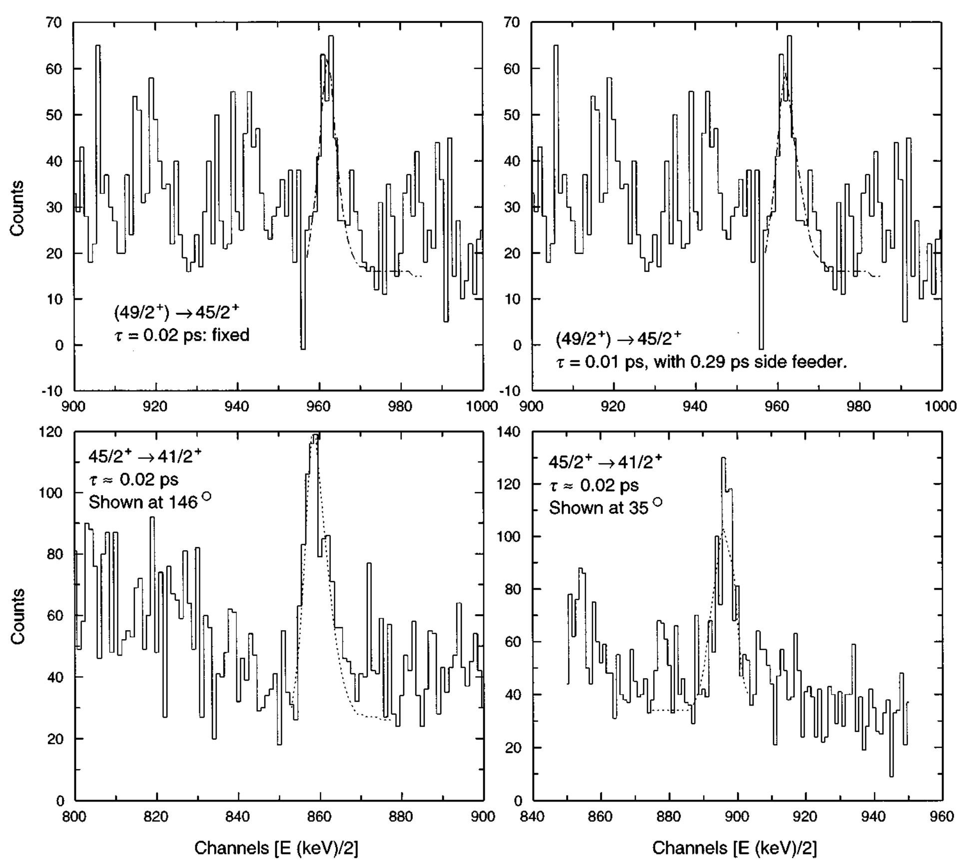

FIG. 5. Shifted lines of very high-spin transitions in ^{83}Y. Line shapes generated from LILIFIT are shown as dashed lines.

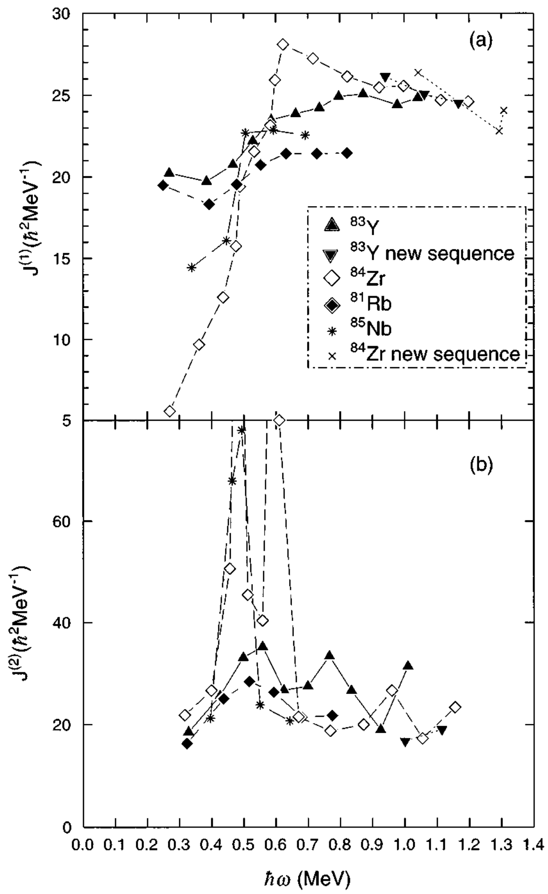

FIG. 6. (a) Kinematic, $J^{(1)}$, and (b) dynamic, $J^{(2)}$, moments of inertia for ^{83}Y and neighboring isotones. Lines are drawn to aid the eye.

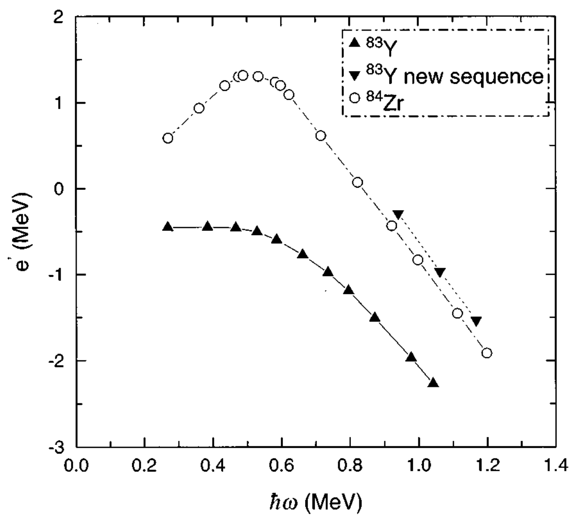

FIG. 7. Single-particle Routhians for ^{83}Y and ^{84}Zr. The Harris parameters used for the reference rotor were $J_0 = 20\hbar^2$/MeV and $J_1 = 0\hbar^4$/MeV^3 from Ref. [10].

try ratios due to the weaker population of these bands and to the very close doublet nature of the 908 and 909 keV lines in the unfavored and favored bands, respectively. One new interband transition, connecting the $(27/2^-)$ to the $25/2^+$ state of the yrast band was found. Two new transitions at 1687 and 1743 keV were found to populate the highest known level of the $\pi = -, \alpha = -1/2$ band. Neither transition was seen in coincidence with the other, and so it is proposed that they both directly populate the 8708 keV level. Intensities could not be obtained for this band due to the very weak population and contamination from strong transitions in ^{80}Sr also produced in the same reaction. In an earlier study [10], it was suggested that the 1416 keV line was, in fact, a quadruplet, with one component also being persisting in the (+,+) band up to high excitation, i.e., to the $(33/2^+ \rightarrow 29/2^+)$ transition. This is also observed in the present data, but careful gating procedures were not sufficient for any firm placement for the other components of the 1416 keV multiplet.

The $(\pi = -, \alpha = +1/2)$ band was extended to a tentative spin and parity of $53/2^-$. Two side-feeding lines at 776 and 1278 keV were reported previously. The level depopulated by the 1278 keV line was found to be populated by a series of transitions. This appears to be a forking of the $(-,+)$ band. One new transition from this branch was found to connect to the high-K band, similar to a situation observed [17] in ^{79}Kr. To date, very little is observed with regards to links of the ''isomeric'' band in ^{83}Y to other bands. Any new connecting transition could be significant to the understanding of their underlying structures.

IV. LIFETIME MEASUREMENTS

Lifetime measurements for short-lived states were obtained from line shape analysis observed in the forward and backward positioned detectors in Early Implementation Gammasphere. Details of the geometry have been noted in Sec. II. The program LILIFIT [18,19] was used for the line shape analysis. Electronic and nuclear components of the stopping powers were calculated with the code TRIM86 [20], using the most recent and complete version of stopping power data. A Monte Carlo simulation traced the detailed history of 10^4 ions through both the target and the Au backing taking into account both longitudinal and lateral straggling. Efficiencies of the detectors, along with the finite solid angles were also taken into account. Direct feeding from within the band of interest was used for the fitting along with side-feeding cascades [21] populating each state.

Lifetimes for levels in ^{83}Y could be measured in the (+,+) band and in the $(+,-)$ band. The results are summarized, along with inferred transition strengths and quadrupole moments, in Table III. Some experimentally observed line shapes with the simulated line shape fits from LILIFIT are illustrated in Fig. 4. They range from very short lifetimes in the (+,+) band (below 0.1 ps for the $37/2^+$ state) shifted nearly completely in flight, to where the major portion of the decay occurs after the recoil nucleus is stopped (0.60 ps for the $23/2^+$ state) in the $(+,-)$ band. Unfortunately, the statistics of transitions in the $\pi = -$ bands were not sufficient to permit reliable line shape analysis. The highest levels in the (+,+) band tend to be nearly completely shifted and hence also do not permit a completely unambiguous DSA analysis. Nevertheless, these lines reveal new information in a qualitative sense, as they indicate whether the states in fact appear collective. Figure 5 shows the line shapes for the highest energy transitions obtainable from the angle dependent matrices together with shapes generated from LILIFIT. For the 1966 keV line, there appear to be two components. The most prominent peak is centered at 1921 keV, precisely the Doppler-shifted energy of the 1966 keV line using $V/c=0.028$. The second, ''slower'' component appears to be contributing to some line shape. It was found that if two side-feeding cascades are used for the line shape analysis in LILIFIT and fit simultaneously, one side cascade yields a lifetime of 0.02 ps and the second yields a slower component of 0.28 ps with a reasonable fit. This coincides with a simultaneously fitted lifetime of 0.01 ps for the $(49/2^+)$ state. This suggests that there could be a long-lived state populating the $(49/2^+)$ level and it is tempting to associate this with the 2159 keV transition depopulating the high spin sequence extending to $(59/2^+)$. Qualitatively, the presence of a well-centered centroid at the maximum Doppler shift in energy and a shifted component at lower energy could be consistent with a very short-lived state being fed by a transition from a somewhat longer-lived state. However, the poor statistics did not permit a line shape analysis for the 2159 keV line, or any of the transitions from the cascade it depopulates. A similar line shape analysis is attempted with the 1754 keV line. As with the 1966 keV line, the centroid of the shifted peak corresponds with the maximum Doppler shift. In the back-angled spectrum, there again appears to be a ''slow component'' to the line shape, similar to the case for the 1966 keV line. In this case however, the 1966 keV line is more intense relative to the ''fast component.'' In the forward-angled spectrum, the ''slow component'' is less clearly defined. When the upper limit of 0.04 ps for the 1966 keV direct feeder was used to fit this peak, the best fit lifetime value for the 1754 keV line was 0.02 ps. Again, an attempt was made to use two side-feeding cascades for the feeding corrections [taking into account side-feeding into the $(49/2^+)$ state]. Similarly, a fast side feeder (0.03 ps) and a slow feeder (0.32 ps) gave the best fit. An attempt was made to fit all four feeder cascades at once with the same results. The 1606 keV line was then fit using 0.02 ps for the direct feeding, and this procedure was reiterated down the cascade. The results are summarized in Table III, along with all measured lifetimes and deduced quantities. When viewing this table, it must be remembered to view those lifetime values below 0.1 ps with extreme caution due to the unreliability of attempting line shape analysis of these fully to nearly fully shifted lines. However, using these lifetimes for the feeding of the states below seems reasonable. The LILIFIT results for those transitions did show much sensitivity to the variations in feeding times below 0.2 ps. Also, the lifetimes of the high-lying states do seem to fit well within this range. The fact that the highest lines retain a fast component appears to indicate that the states themselves have relatively short lifetimes and have not lost collectivity.

V. DISCUSSION

A. Cranked shell model analysis

The kinematic and dynamic moments of inertia, J^1 and J^2, for the $(+,+)$ band in ^{83}Y are displayed in Fig. 6, along with those for neighboring isotones ^{81}Rb [22,23], ^{85}Nb [24], and ^{84}Zr [2], for comparison. Also, the moments of inertia for the very high spin sequence of the three transitions found for both ^{83}Y and ^{84}Zr are represented. The most obvious feature is the low $J^{(1)}$ values at low rotational frequencies for ^{84}Zr that undergo very rapid alignment, in contrast to the odd-Z nuclei where the odd proton polarizes the core to a higher moment of inertia. The alignments in ^{84}Zr were explained [25] by the alignment of two-$g_{9/2}$ quasiprotons at $\hbar\omega=0.50$ MeV followed by a $g_{9/2}$ quasineutron alignment at $\hbar\omega=0.60$ MeV. This is seen dramatically in the $J^{(2)}$ plot in Fig. 6(b). After the alignments, the high spin behavior of ^{84}Zr has been described [25] in terms of rigid rotation. In contrast to ^{84}Zr, the alignment pattern for all the odd-Z isotones have been interpreted [10,22,24] as initial $g_{9/2}$ quasineutron alignments followed by a quasiproton alignment. This is supported by blocking arguments, comparisons with predicted crossing frequencies [10], and systematics.

The behavior of the very three highest lying transitions in ^{83}Y is quite interesting. The kinematic moments of inertia align themselves nearly perfectly with those for the highest lying states of the yrast band in ^{84}Zr and appear to be rotational in character. In contrast, the new transitions found in ^{84}Zr do not exhibit any regular rotational behavior and are therefore probably single particle in nature, caused by alignments of several nucleons at high spin. The comparison between the highest yrast states in ^{84}Zr and the new ^{83}Y states is further enhanced by examining the experimental single-particle Routhians in Fig. 7. Indeed, it appears as though the new ^{83}Y transitions do not at all follow that same structure as the regular ^{83}Y yrast band, instead they seem to be coming from an entirely new structure or orbital very closely related to the highest observed spin states in ^{84}Zr. The $J^{(1)}$ values for the yrast bands of ^{84}Zr and ^{83}Y do appear to be converging to the same value of around $25\hbar^2\mathrm{MeV}^{-1}$. The odd-$Z$ isotones of ^{83}Y seem to be converging to a lower value, but not enough is known at higher spins to continue a fair comparison. A point worth mentioning is that the final observed transition, that appears to be continuing the yrast sequence in ^{83}Y could be the beginning of a new alignment [see Fig. 6(b)], but not enough data are available to make a definite conclusion concerning its nature.

Single-particle alignments and dynamic moments of inertia for the $(-,+)$ bands of ^{83}Y and ^{81}Rb [23] are shown in Figs. 8(a) and (b). The alignments (and therefore also $J^{(1)}$ and $J^{(2)}$) exhibit a trend for steadily decreasing values at the highest spins. Similar behavior has recently [26] been interpreted as band termination in ^{113}I. It seems very likely that band termination is observed for the first time in ^{83}Y for the negative parity band due to the nucleons being aligned to the maximum spin possible using the $g_{9/2}, f_{5/2}, p_{1/2}$ orbitals. The lowest 1qp negative parity bands in this region are explained [10] in terms of $f_{5/2}-p_{3/2}$ mixing. In this circumstance, neither proton nor neutron crossings are blocked, and since, in the mass 80 region they often occupy the same major shells, proton and neutron alignments can occur at similar rotational frequencies. Shapes are dependent on the relative position of suborbitals within the $g_{9/2}$ shell and so the polarized shape depends on whether protons or neutrons align. Quasiproton alignments are expected to drive the system towards more collective prolate shapes and quasineutron alignments to-

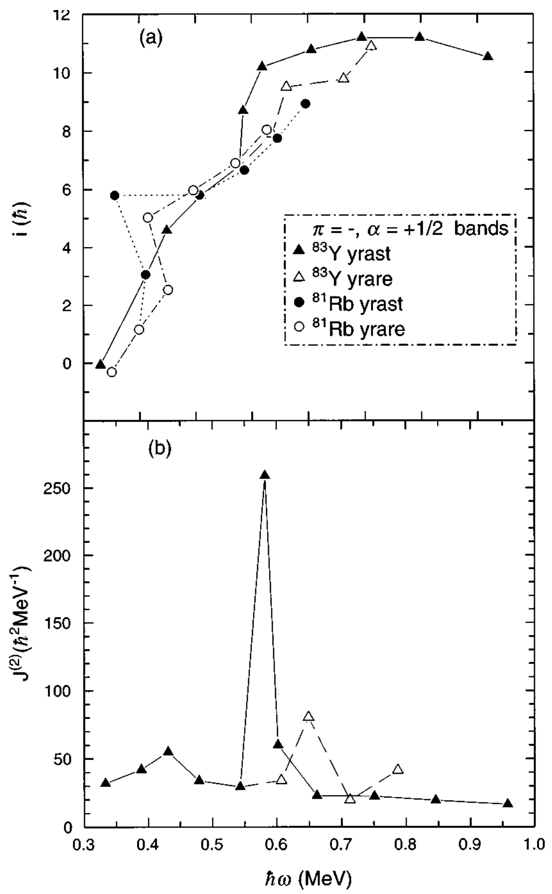

FIG. 8. (a) Single-particle alignments and (b) dynamic moments of inertia, $J^{(2)}$ for the $\pi=-,\alpha=+1/2$ bands in ^{83}Y and ^{81}Rb. The Harris parameters used for the reference rotor were $J_0=20\hbar^2/$MeV and $J_1 = 0\hbar^4/\mathrm{MeV}^3$ from Ref. [10].

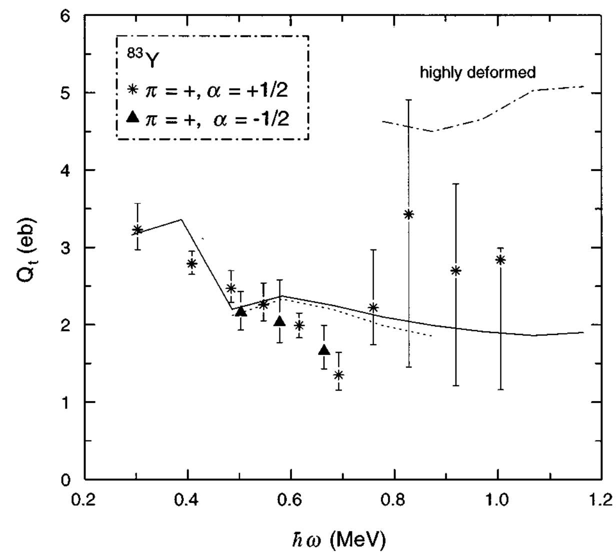

FIG. 9. Transition quadrupole, $|Q_t|$, moments for the $\pi=+$ bands in ^{83}Y. The solid line corresponds to the predicted yrast configuration for the $\alpha=+1/2$ signature, starting with $\beta_2\approx 0.33$ and dropping to $\beta_2\approx 0.22$ around $\hbar\omega\approx 0.5$ MeV. The short-dashed line shows the similar deformation values after the band crossing for the $\alpha=-1/2$ band. The long-short dashed line near the top of the figure shows the Q_t values corresponding to the configuration predicted with a deformation value of $\beta_2\approx 0.45-0.50$.

wards the collective oblate side. This has been discussed [22] in connection with the $(-,+)$ band forking in ^{81}Rb where it was mentioned that due to the closeness in the crossing frequencies it could not be definitively determined which crossing (proton or neutron) was associated with which 3qp band. Figure 8 shows that the alignments of the two bands follow each other very closely. In ^{83}Y, a similar forking has been observed. The single-particle aligned angular momentum for the new band follows very closely both forks of the $(-,+)$ bands in ^{81}Rb, indicating a weaker band interaction than for the band crossing observed in the yrast band. The alignment sequence for ^{83}Y was suggested to be first a proton alignment at $\hbar\omega=0.43$ MeV, followed by a sharp neutron alignment at $\hbar\omega=0.58$ MeV. We suggest, due to a predicted lower crossing frequency for neutrons, that the sharp alignment taking place at $\hbar\omega=0.58$ MeV is due to a $g_{9/2}$ neutron crossing and that the alignment at $\hbar\omega=0.65$ MeV is probably a $g_{9/2}$ proton crossing. Measurements of g factors would clarify the situation. The earlier interpretation [10] had been that the high-K band was actually responsible for the forking. However, a systematic comparison [4] with other nuclei in this region, such as ^{77,79,81}Br, ^{79,81,83}Rb, and ^{79}Kr, some of which have forkings of the negative parity bands *and* the presence of high-K bands, suggested that this is not the case. The presence of the new forking in ^{83}Y supports this and suggests that the high-K band in ^{83}Y has a similar microscopic structure as those in other nuclei. There have been g-factor measurements [7] indicating a complex bandhead configuration involving active protons and neutrons. Since neither proton nor neutron crossing is blocked, there seems to be no reason to exclude such a configuration.

B. Transition strengths

Transition strengths were calculated from lifetimes and their inferred quadrupole moments which were extracted in this experiment have been summarized in Table III. Included with the new lifetimes are those from previous measurements for comparison. An upper limit of 0.10 ps has been assigned to all such lifetimes since that is the value which can be known with some certainty. Taking these values as reasonable estimates, it is evident that a high degree of collectivity persists to the highest spin states. The quadrupole moments are plotted in Fig. 9, together with those of predicted values to be discussed in Sec. V C.

This work presents the first measurement of lifetimes in the $(+,-)$ band. Results are summarized in Table III and the Q_t moments are plotted in Fig. 9. They closely follow those of the favored band within the frequency range for which they could be measured. Reduced $B(M1)$ strengths for interband links between the unfavored and favored bands were also calculated assuming a mixing ratio of 0.1, as has been done in previous work [27]. In the case of transitions where intensities could not be measured and reliably normalized, namely for the 1025 and 1022 keV γ-ray lines, branching ratios were obtained from gate combinations from higher levels. It is found that the branching ratios for the new $\Delta I=1$ transitions are lower than those of that for the previously known 1037 keV line, although the intensity is roughly half of its previous value. The $B(M1)$ strengths for the $\Delta I=1$ transitions, which could be determined [10] from the new lifetime measurements are found to be quite weak.

C. Woods-Saxon calculations and lifetime comparisons

Woods-Saxon-Bogolyubov calculations [29,30] were carried out to investigate the high-spin structure of ^{83}Y using the Woods-Saxon model discussed in Ref. [28]. The monopole pairing force was assumed and the cranking approximation was used to describe the rotation. The total Routhians were calculated at each β_2 and γ in the mesh and minimized with respect to the hexadecapole deformation β_4.

Examples of calculated total Routhian surfaces (TRS's) in the (β_2,γ) contour plots for ^{83}Y have been presented [10] previously. The results can be briefly summarized as follows: For the 1qp bands, the $(+,+)$ configuration had $\beta_2=0.33$ and $\gamma=-7°$, and are quite γ soft. The unfavored configuration was very similar but with a more triaxial shape with $\gamma=-24°$. More recent calculations using a newer version of the TRS codes installed at Notre Dame suggest that the favored configuration is actually more triaxial than for the unfavored, but in this frequency domain, the large gamma softness allows for considerable flexibility in definite deformation parameters. After a neutron alignment, both configurations were predicted to have smaller deformations ($\beta_2=0.22$) and highly oblate shapes with $\gamma=-57°$. At higher rotational frequencies, above $\hbar\omega=0.680$ MeV, a secondary minimum is found at nearly prolate $\beta_2\approx 0.45-0.50$, and becomes yrast at $\hbar\omega=1.165$.

With the present lifetime measurements, it is possible to compare experimental results for the positive parity bands with predictions from the cranked Woods-Saxon-Bogolyubov calculations. A comparison of the quadrupole moments inferred from the lifetime measurements with those predicted from the TRS calculations is presented in Fig. 9. The equations necessary to calculate quadrupole moments from the deformation parameters are presented in Refs. [31,32]. The expression for Q_t in terms of γ is valid for high spins and also reflects pure geometrical shapes; therefore, structure and band mixing effects are ignored. The deformation parameters used for the calculations are those calculated from the newer versions of the TRS codes, and do not differ significantly from the previous results. Lifetimes in the $(+,-)$ band are known only for the alignment region and higher, therefore only predicted values for the relevant frequency range are shown. Although the experimental values are somewhat less than those predicted, the trend towards decreasing moments is reproduced experimentally. In addition, the predicted agreement in Q_t between favored and unfavored bands is reproduced very well and is consistent with moderately deformed oblate shapes.

The quadrupole moments for the highest rotational frequencies from the $(+,+)$ band have quite large uncertainties resulting from the uncertainties in fitting line shapes for the highly shifted peaks. Predicted quadrupole moments for the highly deformed shape with $\beta_2\sim 0.45$ shown at the top with the short-long–dashed line lie higher than the probable experimental lifetimes. Values corresponding to shorter lifetimes are subject to much more uncertainty at this level. The upper limits on the lifetimes yield quadrupole moment values that are consistent with the collective oblate shapes predicted by the Hartree-Fock-Bogolyubov calculations.

VI. SUMMARY

The observation of extremely high spin states up to $I=(59/2^+)$ and $E_x = 19.475$ MeV in ^{83}Y and the resolution of very close doublets was made possible with the excellent statistics in triples data provided by the Early Implementation Gammasphere spectrometer. The previously published level scheme of ^{83}Y was extended to a probable spin state of $59/2^+$. A new sequence of three transitions was placed and found to exhibit a very similar behavior to the highest observed levels in the yrast ground state band in the $N=44$ isotone ^{84}Zr. This similarity is observed in a comparison of moments of inertia and single-particle Routhians. There is some evidence for the observation of the first transition of a superdeformed band in ^{83}Y based on a comparison with the superdeformed band in ^{84}Zr. A side-feeding transition previously reported in the negative parity favored band was found to be the first transition of a fork, due probably to an alignment of different quasiparticles than the ones responsible for the alignment in the more strongly populated cascade. The new band exhibits an alignment at a somewhat higher rotational energy. It is not clear which of the quasiparticles are involved in the alignments. Future g-factor measurements would clarify the situation. The presence of this forking and of the first transition found to feed into the high-K band, underlines the similarity of the structures of high-K bands found in many isotopes in the A $\approx$80 region.

New lifetime measurements in the unfavored positive parity band show the data to be consistent with Hartree-Fock-Bogolyubov calculations showing moderate oblate deformation with $\beta_2=0.22$ and $\gamma\approx-50°$. Several new transitions connecting the unfavored to the favored band were found, due to the excellent resolving power of Gammasphere. Lifetime measurements show their $B(M1)$ strengths to be very weak. The theoretical calculations reveal that the transition quadrupole moments for both positive parity signature partners should be quite similar and gradually decreasing with increasing spin. Within uncertainties, this appears to be consistent with our observations. What is qualitatively clear is that the yrast sequence does not seem to be losing collectivity into a single-particle band termination as the maximum spin in the fp-g shell is reached. Near fully shifted line shapes were compared with simulations and shown to be consistent with collectivity persisting up to $(49/2^+)$.

ACKNOWLEDGMENTS

This research was supported by the NSF under Grant No. PHY94-02761 and by the DOE under Contract No. W-31-109-ENG-38. We would like to thank the Gammasphere and the LBNL support staff for their encouragement and assistance.

[1] C. Baktash, D.M. Cullen, J.D. Garrett, C.J. Gross, N.R. Johnson, W. Nazarewicz, D.G. Sarantites, J. Simpson, and T.R. Werner, Phys. Rev. Lett. **74**, 1946 (1995).

[2] H.-Q. Jin, C. Baktash, M.J. Brinkman, C.J. Gross, D.G. Sarantites, I.Y. Lee, B. Cederwall, F. Cristancho, J. Döring, F. E. Durham, P.-F. Hua, G.D. Johns, N. Korolija, D.R. LaFosse, E. Landulfo, A.O. Macchiavelli, W. Rathbun, J.X. Saladin, D.W. Stracener, S.L. Tabor, and T.R. Werner, Phys. Rev. Lett. **75**, 1471 (1995).

[3] D.R. LaFosse, P.F. Hua, D.G. Sarantites, C. Baktash, Y.A. Akovali, M. Brinkman, B. Cederwall, F. Cristancko, J. Döring, C.J. Gross, H.-Q. Jin, M. Korolija, E. Landulfo, I.Y. Lee, A.O. Macchiavelli, M.R. Maier, W. Rathburn, J.X. Saladin, D.W. Stracener, S.L. Tabor, A. Vander Mollen, and T.R. Werner, Phys. Lett. B **354**, 34 (1995).

[4] S.L. Tabor and J. Döring, Phys. Scr. **T56**, 175 (1995).

[5] T.D. Johnson, F. Cristancho, C.J. Gross, M. Kabadiyski, K.P. Lieb, D. Rudolph, M. Weiszflog, T. Burkardt, J. Eberth, and S. Skoda, Z. Phys. A **347**, 285 (1994).

[6] R. Sahu and S.P. Pandya, Nucl. Phys. **A529**, 20 (1991).

[7] K. Bharuth-Ram, J. Billowes, C.J. Gross, J. Heese, K.P. Lieb, J. Eberth, and S. Skoda, Phys. Lett. B **252**, 540 (1990).

[8] M.S. Rapaport, C.F. Liang, and P. Paris, Phys. Rev. C **36**, 303 (1987).

[9] C.J. Lister, B.J. Varley, W. Fieber, J. Heese, K.P. Lieb, E.K. Warburton, and J.W. Olness, Z. Phys. A **329**, 413 (1988).

[10] F. Cristancho, C.J. Gross, K.P. Lieb, D. Rudolph, Ö. Skeppstedt, M.A. Bentley, W. Gelletly, H.G. Price, J. Simpson, J.L. Durell, B.J. Varley, and S. Rastikerdar, Nucl. Phys. **A540**, 307 (1992).

[11] F. Cristancho, K.P. Lieb, J. Heese, C.J. Gross, W. Fieber, Th. Osipowicz, S. Ulbig, K. Bharuth-Ram, S. Skoda, J. Eberth, A. Dewald, and P. Von Brentano, Nucl. Phys. **A501**, 118 (1989).

[12] Gammasphere Report LBL-PUB-5202; I.Y. Lee, Nucl. Phys. **A520**, 641C (1990).

[13] T. Lauritsen (private communication).

[14] J.A. Kuehner *et al.*, Proceedings of the International Conference on Nuclear Structure at High Angular Momentum, Ottawa, 1992 (Report No. AECL-10613), p. 43.

[15] B. Crowell (private communication).

[16] B. Crowell, M.P. Carpenter, R.G. Henry, R.V.F. Janssens, T.L. Khoo, T. Lauritsen, and D. Nisius, Nucl. Instrum. Methods Phys. Res. A **355**, 575 (1995).

[17] G.D. Johns, J. Döring, J.W. Holcomb, T.D. Johnson, M.A. Riley, G.N. Sylvan, P.C. Womble, V.A. Wood, and S.L. Tabor, Phys. Rev. C **50**, 2786 (1994).

[18] H. Emling *et al.*, in *Proceedings of the Twenty-Second School on Physics*, Zakopane, Poland, 1987, edited by R. Broda and Z. Stachura (Instytut Fizyki Jadrowej w Krakowie Report No. IFJ 1956/PL), p. 151.

[19] H. Emling, I. Ahmad, P.J. Daly, B. Dichter, M. Drigert, U. Garg, Z.W. Grabowski, R. Holzmann, R.V.F. Janssens, T.L. Khoo, W.C. Ma, M. Piiparinen, M.A. Quader, I. Ragnarsson, and W.H. Trzaska, Phys. Lett. B **217**, 33 (1989).

[20] J.F. Ziegler, J.P. Biersack, and V. Littmark, in *The Stopping and Range of Ions in Solids* (Pergamon, New York, 1985).

[21] H. Emling, E. Grosse, R. Kulessa, D. Schwalm, and H.J. Wollersheim, Nucl. Phys. **A419**, 187 (1984).

[22] S.L. Tabor, P.D. Cottle, C.J. Gross, U.J. Hüttmeier, E.F. Moore, and W. Nazarewicz, Phys. Rev. C **39**, 1359 (1989).

[23] J. Döring, R. Schwengner, L. Funke, H. Rotter, G. Winter, B. Cederwall, F. Liden, A. Johnson, A. Atac, J. Nyberg, and G. Sletten, Phys. Rev. C **50**, 1845 (1994).

[24] C.J. Gross, K.P. Lieb, D. Rudolph, M.A. Bentley, W. Gelletly, H.G. Price, J. Simpson, D.J. Blumenthal, P.J. Ennis, C.J. Lister, Ch. Winter, J.L. Durell, B.J. Varley, Ö. Skeppstedt, S. Rastikerdar, Nucl. Phys. **A535**, 203 (1991).

[25] H.G. Price, C.J. Lister, B.J. Varley, W. Gelletly, and J.W. Olness, Phys. Rev. Lett. **51**, 1842 (1983).

[26] M.P. Waring, E.S. Paul, C.W. Beausang, R.M. Clark, R.A. Cunningham, T. Davinson, S.A. Forbese, D.B. Fossan, S.J. Gale, A. Gizon, J. Gizon, K. Hauschild, I.M. Hibbert, A.N. James, P.M. Jones, M.J. Joyce, D.R. LaFosse, R.D. Page, I. Ragnarsson, H. Schnare, P.J. Sellin, J. Simpson, P. Vaska, R. Wadsworth, and P.J. Woods, Phys. Rev. C **51**, 2427 (1995).

[27] T.D. Johnson, J.W. Holcomb, P.C. Womble, P.D. Cottle, S.L. Tabor, F.E. Durham, S.G. Buccino, and M. Matsuzaki, Phys. Rev. C **42**, 2418 (1990).

[28] W. Nazarewicz, J. Dudek, R. Bengtsson, T. Bengtsson, and I. Ragnarsson, Nucl. Phys. **A435**, 397 (1985).

[29] E.F. Moore, P.D. Cottle, C.J. Gross, D.M. Headly, U.J. Hüttmeier, S.L. Tabor, and W. Nazarewicz, Phys. Rev. C **38**, 696 (1988).

[30] W. Nazarewicz and T. Werner, in *Nuclear Structure of the Zirconium Region*, edited by J. Eberth, R.A. Mayer, and K. Sistemich (Springer-Verlag, Berlin, 1988), p. 277.

[31] P. Ring, A. Hayashi, K. Hara, H. Emling, and E. Grosse, Phys. Lett. **110B**, 423 (1982).

[32] I. Hamamoto and B.R. Mottelson, Phys. Lett. **132B**, 7 (1983).